SETSCI Conference Indexing System,
Volume 3 (2018), 933-938

ISAS 2018-Winter
2nd International Symposium on Innovative Approaches in Scientific Studies
November 30 – December 2, 2018, Samsun, Turkey

Computational studies on the vanadocene dithiocarbamate complexes

Sultan ERKAN[1*+]

[1*]Chemistry and Chemical Processing Technologies, Sivas Cumhuriyet University
*Corresponding author: sultanerkan58@gmail.com
+Speaker: sultanerkan58@gmail.com
Presentation/Paper Type: Oral / Full Paper

Abstract- $[Cp_2V\{S_2CN(CH_2)_4O\}]^+$ and $[(\eta^5\text{-}C_5H_4Me)_2V\{S_2CN(CH_2)_4O\}]^+$ complexes are optimized B3LYP/GEN level (GEN keyword is mean that LANL2DZ basis set for metal atom and 6-31G(d) basis set for S, O, N, C and H atoms) in gas phase. The aim in this study, the molecular structures, some parameters effecting on biological activity and molecular docking toward MOLT-4 cells are calculated by using B3LYP method in the gas phase.

Keywords- *Vanadocene dithiocarbamate, DFT, Biological activities, Molecular docking*

1. Introduction

In the last two decades, vanadocene derivatives have been synthesized with various substituents. These complexes have many advanced biological applications [1]. Increased cytotoxicity has been observed for several vanadocene species which are included as a functional group in the side chains of cyclopentadienyl rings [2,3]. In many studies, antibacterial [4,5] and antifungal properties of metal dithiocarbamates have attracted considerable attention [6]. They found the pesticide application in agriculture [7]. The cationic vanadocene diethyldiadithiocarbamate complex, $[Cp_2V(S_2CNEt_2)]^+$, exhibits a strong spermicidal activity without toxicity or systemic vanadium absorption [8-11]. Computational chemistry allows the acquisition of any data that are not experimentally described.

1. Calculation procedure

In the first step, the geometries of the studied complexes were prepared with GaussView 5.0.8. All calculations were performed in the gas phase using Gaussian IA32W-G09RevA.02 and Gaussian AS64L-G09RevD.01 [12-14]. In the second step, the geometries were completely optimized by the DFT/B3LYP method [15,16]. All geometry optimizations were followed by frequency calculations and no imaginary frequencies were found [17]. DFT/B3LYP is a hybrid method that involves the effects of electron correlation using the general functions of electron density. LANL2DZ basis set for the vanadium atoms and the 6-31G(d) basis set for the other atoms were used. The LANL2DZ basis set is commonly used for atoms beyond the third row of the periodic table. The 6-31G(d) basis set adds d functions to heavy atoms.

2. Results and discussion

2.1. Optimized structures

The investigated complexes are optimized at B3LYP/LANL2DZ/6-31G(d) level in gas phase. The optimized structures are shown in Figure 1. The main difference between the two complexes is the methyl groups on the Cp ligands.

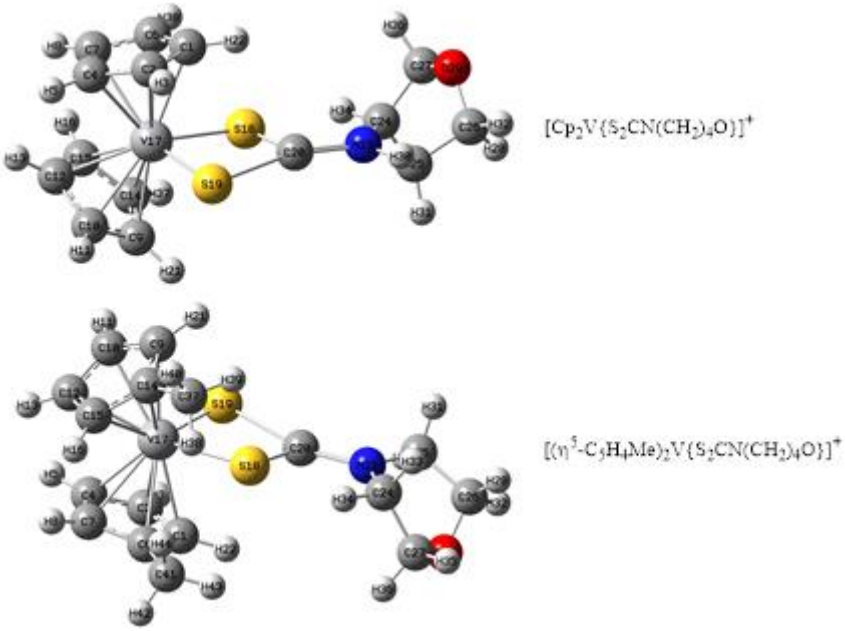

Figure 1. The optimized structures of $[Cp_2V\{S_2CN(CH_2)_4O\}]^+$and $[(\eta^5\text{-}C_5H_4Me)_2V\{S_2CN(CH_2)_4O\}]^+$

2.2. Structural parameters of vanadium complexes

The experimentally bond lengths and angles of $[(\eta^5\text{-}C_5H_4Me)_2\{S_2CN(CH_2)_4O\}]^+$ are compared with calculated structural parameters. The structural parameters are calculated at the B3LYP/LANL2DZ/6-31G(d,p) level in gas phase. The experimental and calculated structural parameters are given in Table 1.

Table 1. Selected bond lengths (Å) and bond angles (°) for (5) and (6)

$[(\eta^5\text{-}C_5H_4Me)_2V\{S_2CN(CH_2)_4O\}]^+$	**Exp.**	**Calc.**	**$[Cp_2V\{S_2CN(CH_2)_4O\}]^+$**	**Calc.**
$V–Cg_1$[a]	1.9548 Å	2.1936 Å	$V–Cg_1$[a]	2.0812 Å
$V–Cg_2$[a]	1.9579 Å	2.2595 Å	$V–Cg_2$[a]	1.9474 Å
V–S19	2.4821 Å	2.0937 Å	V–S19	2.5790 Å
V–S18	2.4904 Å	2.5553 Å	V–S18	2.1017 Å
$Cg_1–V–Cg_2$[a]	133.66°	135.91°	$Cg_1–V–Cg_2$[a]	129.91°
S1–V–S2	70.39°	92.26°	S1–V–S2	92.48°

[a]Cg denotes center of gravity of the five-membered ring.

When Table 1 are examined, the calculated bond lengths of V–Cg are less than the experimental data. In additional, structural parameters of $[(\eta^5\text{-}C_5H_4Me)_2V\{S_2CN(CH_2)_4O\}]^+$ are more than $[Cp_2V\{S_2CN(CH_2)_4O\}]^+$. This may be due to the steric effect of methyl groups added to the Cp ligand

2.3. IR spectra

Bands in the IR spectrum of complexes consist of multiple vibrational passages. Some of the vibrational transitions that make up a band are violent and some are weak. The highly vibrated oscillatory transition contributes more to the band. These vibration modes are known as basic vibration modes or harmonic frequencies. The vibration modes in the IR spectrum for $[Cp_2V\{S_2CN(CH_2)_4O\}]^+$ and $[(\eta5\text{-}C_5H_4Me)_2V\{S_2CN(CH_2)_4O\}]^+$ are given in Figure 2. The assignment of the bond stretching were presented in Table 2.

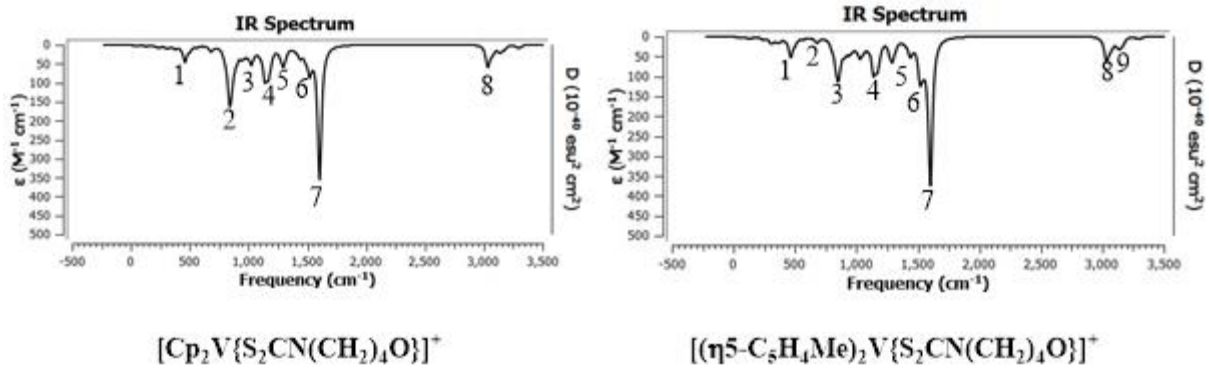

$[Cp_2V\{S_2CN(CH_2)_4O\}]^+$ $[(\eta5\text{-}C_5H_4Me)_2V\{S_2CN(CH_2)_4O\}]^+$

Figure 3. IR spectra of the mentioned complexes.

Table 2. The labeled bond stretching (cm^{-1}) corresponding to the numbered IR spectra for investigated complexes

$[Cp_2V\{S_2CN(CH_2)_4O\}]^+$			$[(\eta^5\text{-}C_5H_4Me)_2V\{S_2CN(CH_2)_4O\}]^+$		
Mode	**Freq.**	**Assign.**	**Mode**	**Freq.**	**Assign.**
1	459.4	νV-S	1	464.9	νV-S
2	834.0	Wagging C_{aro}-H	2	848.7	Wagging C_{aro}-H
3	1023.8	νC-S+νC$_{ali}$-C$_{ali}$	3	1025.3	νC-S+νC$_{ali}$-C$_{ali}$
4	1138.0	νC-N+νO-C$_{ali}$	4	1138.4	νC-N+νO-C$_{ali}$
5	1294.7	νC=N+Twisting Cali-H	5	1292.6	νC=N+Twisting Cali-H
6	1520.8	Bending C$_{ali}$-H	6	1520.5	Bending C$_{ali}$-H
7	1603.9	νC=N	7	1601.7	νC=N
8	3036.6	νC-H	8	3035.84	νC-H
			9	3149.4	νC-H

When the vibrational frequencies of the studied complexes were examined to according to bond stretching. The vibrational frequencies of $[Cp_2V\{S_2CN(CH_2)_4O\}]^+$ and $[(\eta5\text{-}C_5H_4Me)_2V\{S_2CN(CH_2)_4O\}]^+$ are similar with each other. Already, the both complexes are structurally similar.

2.4.Quantum chemical descriptors

Biological activity may correlate with the increase and/or decrease of calculated parameters. For example, the biological activity of a chemical species increases with the increase of HOMO, softness and electronegativity. Biological activity decreases with decreasing LUMO energy,

energy gap, hardness and chemical potential. Also, biological activity decreasing of electrophilicity index and increases with increasing of nucleophilicity index. Additionally, ΔN_{max} is corelated with charges of compounds and the biological activity of compound increases with increasing of ΔNmax values. The calculated the quantum chemical descriptors of the compounds in Table 2 are given. In view of this information, according to the parameters in Table 2, the $[Cp_2V\{S_2CN(CH_2)_4O\}]^+$ is biologically more active than the $[(\eta5\text{-}C_5H_4Me)_2V\{S_2CN(CH_2)_4O\}]^+$.

Table 2. The calculated quantum chemical descriptors of the mentioned compounds

	$[Cp_2V\{S_2CN(CH_2)_4O\}]^+$	$[(\eta5\text{-}C_5H_4Me)_2V\{S_2CN(CH_2)_4O\}]^+$
E_{HOMO}*	-6.502	-5.237
E_{LUMO}*	-1.740	-0.152
ΔE*	4.762	5.085
η*	2.381	2.542
σ**	0.420	0.393
χ*	4.121	2.695
CP*	-4.121	-2.695
ω	3.567	1.428
ε	-9.812	-6.851
ΔN_{max}	1.731	1.060
*** is in (eV) unit ** is in (eV^{-1}) unit**		

2.5. Molecular electrostatic potential (MEP) and contour diagrams

Molecular electrostatic potential (MEP) information can visualize the electron density in a molecule. The MEP information shows nucleophilic and electrophilic domains of the specified moles and in part indicates chemical reactivity [18]. In the MEP diagram, the negative regions are considered as nucleophilic centers and reveal electrophilic attack zones (colored in red shades in standard contour diagrams). A positive electrostatic potential is a region of low electron density (blue in standard contour schemes) [19-21]. The contour diagrams of HOMO and LUMO orbitals determine the atoms that will be involved in this task in the case of electron donation and electron retrieval. In this context, MEP information and HOMO and LUMO of the investigated complexes molecular orbital contour diagrams were given in Figure 4.

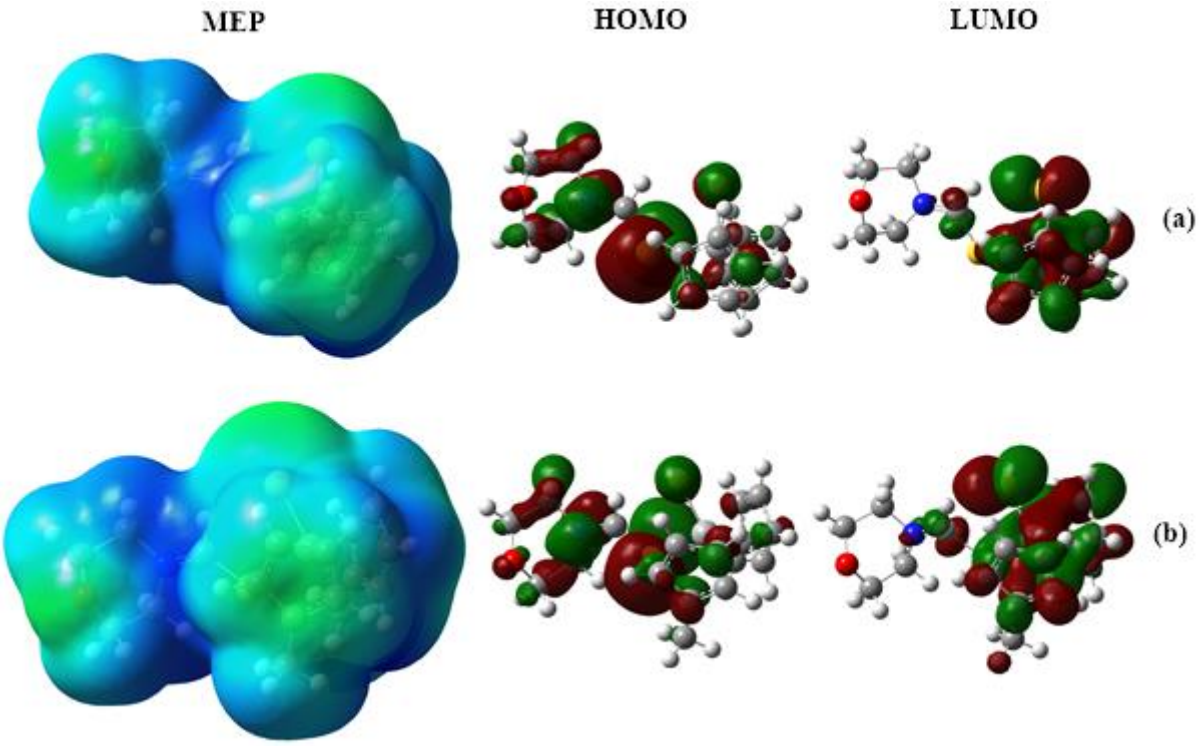

Figure 4. MEP information and contour diagrams of (a) $[Cp_2V\{S_2CN(CH_2)_4O\}]^+$ and (b) $[(\eta5\text{-}C_5H_4Me)_2V\{S_2CN(CH_2)_4O\}]^+$

The light blue region is the region where the electron is missing. The yellow region is a light electron rich region and the green zone is neutral. In addition, the regions where frontier molecular orbitals are concentrated are similar, as shown in Figure 4.

2.6. Molecular docking

Molecular docking studies in computational and bioinformatics chemistry have attracted much attention in recent years for the design, feasibility and development of therapeutically effective chemicals [33]. MOLT-4 showed close affinity with the present PDB template (PDB ID: 2ZTB) which had cytocidal activity against the cell line. For this reason target protein was chosen as the 2ZTB. Molecular docking calculation are made with HEX 8.0.0 program. Binding modes of $[Cp_2V\{S_2CN(CH_2)_4O\}]^+$ and $[(\eta5\text{-}C_5H_4Me)_2V\{S_2CN(CH_2)_4O\}]^+$ with target protein are shown in Figure 5. The binding energy between $[Cp_2V\{S_2CN(CH_2)_4O\}]^+$ with 2ZTB are calculated as 136.60 kJ/mol and the binding energy between $[(\eta5\text{-}C_5H_4Me)_2V\{S_2CN(CH_2)_4O\}]^+$ with target protein are calculated as 140.07 kJ/mol. According to binding energy, $[(\eta5\text{-}C_5H_4Me)_2V\{S_2CN(CH_2)_4O\}]^+$ is more effective against the cell line

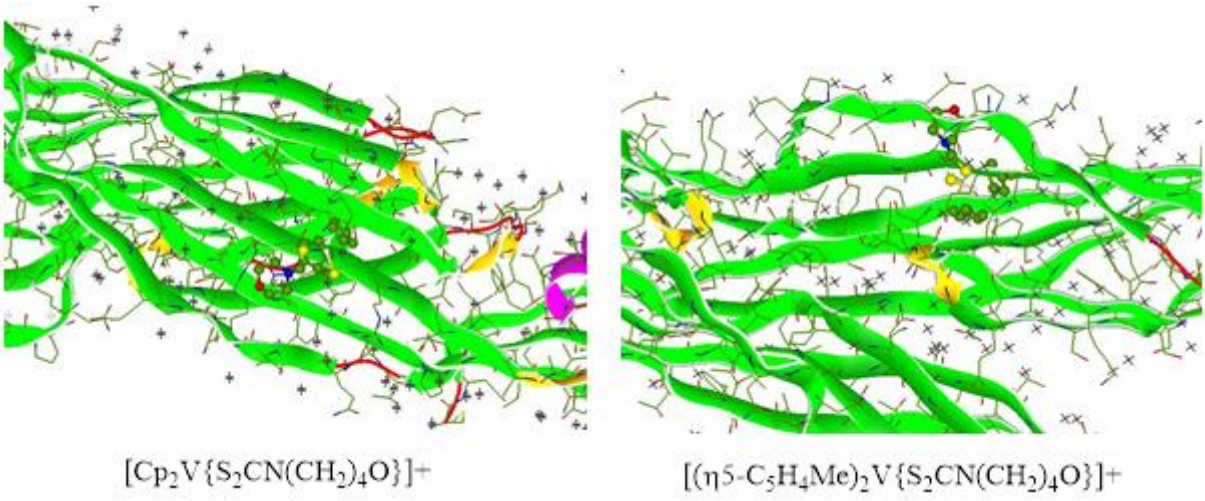

Figure 5. The binding modes of (a) $[Cp_2V\{S_2CN(CH_2)_4O\}]^+$ and (b) $[(\eta5\text{-}C_5H_4Me)_2V\{S_2CN(CH_2)_4O\}]^+$

References

[1] J. Honzíček, J. Vinklárek, Inorg. Chim. Acta 437 (2015) 87–94.
[2] J. Honzíček, I. Klepalová, J. Vinklárek, Z. Padělková, I. Císařová, P. Šiman, M. Řezáčová, Inorg. Chim. Acta 373 (2011) 1–7.
[3] I. Klepalová, J. Honzíček, J. Vinklárek, Z. Padělková, L. Šebestová, M. Řezáčová, Inorg. Chim. Acta 402 (2013) 109–115.
[4] E. Hooward Taylor, E.M. Walker, M. Bartelt, S. Day, A.A. Pappas, Ann. Clin. Lab. Sci. 17 (1987) 171–177.
[5] G. Manoussakis, C. Bolos, L. Ecateriniadou, C. Sarris, Eur. J. Med. Chem. 22 (1987) 421–425.
[6] I.P. Ferreira, G.M. Lima, E.B. Paniago, J.A. Takahashi, C.B. Pinheiro, Inorg. Chim. Acta 423 (2014) 443–449.
[7] A.K. Malik, W. Faubel, Pestic. Sci. 55 (1999) 965–970.
[8] P. Ghosh, S. Ghosh, O.J. D'Cruz, F.M. Uckun, J. Inorg. Biochem. 72 (1998) 89–98.
[9] O.J. D'Cruz, F.M. Uckun, Contraception 72 (2005) 146–156.
[10] O.J. D'Cruz, F.M. Uckun, Toxicol. Appl. Pharmacol. 170 (2001) 104–112.
[11] O.J. D'Cruz, B. Waurzyniak, F.M. Uckun, Contraception 64 (2001) 177–185.
[12] R.D. Dennington II, T.A. Keith, J.M. Millam, GaussView 5.0, Wallingford, CT, 2009.
[13] M. J. Frisch et al., Gaussian, Inc., Wallingford CT, 2009.
[14] M. J. Frisch et al., Gaussian, Inc., Wallingford CT, 2010.
[15] A.D. Becke, J. Chem. Phys. 98 (1993) 5648.
[16] C. Lee, W. Yang, R.G. Parr, Phys. Rev. B 37 (1988) 785.
[17] S. Güveli, N. Özdemir, T. Bal-Demirci, B. Ülküseven, M. Dinçer, Ö. Andaç, Polyhedron 29 (2010) 2393.
[18] M. Wagener, J. Sadowysky, J. Gasteiger, J. Am. Chem. Soc., 117 (1995) 7769–7775.
[19] Jayaraman Jayabharathi, Venugopal Thanikachalam, Marimuthu Venkatesh Perumal, Natesan Srinivasan, Fluorescence resonance energy transfer from a bio-active imidazole derivative 2-(1-phenyl-1Himidazo[4,5-f][1,10]phenanthrolin-2- yl)phenol to a bioactive indoloquinolizine system, Spectrochimica Acta Part A, 79 (2011) 236–244.
[20] G.C. Muscia, Synthesis trypanocidal activity and molecular modeling studiesof 2-alkylaminomethylquinoline derivatives, European Journal of Medicinal Chemistry, 46 (2011) 3696-3703.
[21] P.S. Kushwaha, P.C. Mishra, Int. J. Quant. Chem., 76 (2000) 700